Hybrid electrodynamics and kinetics simulation for electromagnetic wave propagation in weakly ionized hydrogen plasmas

Qiang Chen and Bin Chen[*]

National Key Laboratory of Electromagnetic Environment and Electro-optical Engineering, PLA University of Science and Technology,
Nanjing 210007, People's Republic of China

In this paper, a hybrid electrodynamics and kinetics numerical model based on the finite-difference time-domain method and lattice Boltzmann method is presented for electromagnetic wave propagation in weakly ionized hydrogen plasmas. In this framework, the multicomponent Bhatnagar-Gross-Krook collision model considering both elastic and Coulomb collisions and the multicomponent force model based on the Guo model are introduced, which supply a hyperfine description on the interaction between electromagnetic wave and weakly ionized plasma. Cubic spline interpolation and mean filtering technique are separately introduced to solve the multiscalar problem and enhance the physical quantities, which are polluted by numerical noise. Several simulations have been implemented to validate our model. The numerical results are consistent with a simplified analytical model, which demonstrates that this model can obtain satisfying numerical solutions successfully.

PACS number(s): 47.11.−j, 41.20.Jb, 52.25.Dg

I. INTRODUCTION

The complicated behavior of electromagnetic wave propagation in weakly ionized plasma gas is becoming more and more important because of the recent fast development of plasma stealth technique (PST) [1,2]. As a kind of new concept stealth technique, the PST uses magnetized or unmagnetized cold plasma gas to avoid being detected by radar systems. The PST has a series of advantages, such as wideband absorbing ability, high absorbing efficiency, and low cost. In addition, the shape of protected objects should not be modified. All these advantages make the PST the focus of most researchers in related areas. This situation will continue because of the rapid development of practical PST [3,4]. As an essential fundamental problem in PST, the basic physical process of electromagnetic wave propagation in weakly ionized plasma gas consists of many extremely complex transport phenomena, such as electron-molecule or ion-molecule collisions, electron-ion collisions, and interactions between self-consistent field and charged particles, even more so when boundary conditions and plasma configurations are so complex that analytical solutions are out of the question [5–7]. For the purpose of PST design and other complicated plasma science problems, several different numerical methods have been implemented [8–12].

At the beginning of research on plasma physics, theoretical analysis played an essential role as a large number of important results had been acquired by the methods of single charged particle dynamics, magnetohydrodynamics (MHD), and Vlasov-Maxwell kinetics [5–7]. With the development of plasma physics, however, problems were becoming more and more complicated, containing complex collisions and nonlinear coupling interactions with multiple degrees of freedom, and raising a big challenge in theory to describe the properties of the plasma phenomena. Since the mid-1900s, experimental plasma physics has had continual development, even when theoretical analysis encountered obstacles. Many related fields, such as astrophysics, nuclear fusion technique,

and laser acceleration technique, have been well served by these significant plasma experiments [13,14]. Though the experimental methods have achieved great success, they cannot solve all problems in plasma physics and the costs of most plasma experiments are too expensive. The huge demands in experiments and many other fields require much more interaction laws and accurate results for all kinds of conditions. Numerical simulation, with the development of computer technique and computational physics, supplies a powerful and accurate tool in this regime. Using various numerical simulation methods, a series of significant results have been achieved [8,9].

Generally speaking, there are two kinds of methods that seem to be most popular in plasma numerical simulation: macroscopic methods based on the MHD and microscopic methods based on the charged particle dynamics. In macroscopic simulation, plasmas are treated as continuum media and the basic mathematic model consists of Navier-Stokes equations and Maxwell equations [15,16]. Finite element method (FEM), finite difference method (FDM), and finite volume method (FVM) are three main numerical methods for solving the partial differential equations [17]. With these methods, the MHD simulation has been widely used, especial in astrophysics and magnetic confinement fusion. In microscopic simulation, the dynamics of single particle and the statistical fluctuation are under consideration, and the basic mathematic models are Hamiltonian canonical equations and Maxwell equations. With microscopic results, macroscopic physical quantities could be acquired by statistical analysis. The most famous numerical method of microscopic simulation is one called particle in cell (PIC), which is a kind of simplified molecular dynamics. Using the PIC technique, a large area of plasma problems have been simulated, including nuclear fusion, gas discharge, and free electron laser [8–11]. Though the macroscopic and microscopic simulations have been widely used in computational plasma physics, several intrinsic disadvantages limit their further development in more complicated problems, such as the continuum media hypothesis in macroscopic model, computational resource restraints, and limitation in multiscale simulations. As a

---

[*]emcchen@163.com

combination of the macroscopic and microscopic methods and the new development of physical kinetics theory, the mesoscopic methods based on Boltzmann equation supply a useful and accurate tool to explore new areas in computational plasma physics.

Recently, an essential mesoscopic numerical method called the lattice Boltzmann method (LBM) has been used as an alternative for the simulation of partial differential equations [18,19]. At first the LBM was designed for hydrodynamics simulation based on kinetics model, then had been rapidly and widely developed in almost all fields of physics, even in chemistry, biology, geosciences, economics, and several other extended fields, for its clear physical connotation, succinct schemes, and efficient computational ability [18–41]. In fact, at the beginning of the research, S. Succi *et al.* had introduced the LBM into the MHD equations simulation [21]. In that simulation, plasmas were described by macroscopic Navier-Stokes equations and magnetic diffusion equations, and the LBM as an efficient alternative for macroscopic hydrodynamics simulation was proved successfully. Later on, several other LBM models had been developed for MHD, such as the work by D. O. Martinez *et al.* [24], one of the first three-dimensional (3D) LBM models for MHD by Osborn [35], the 3D LBM models for turbulent MHD by Fogaccia *et al.* [27], the vector LBM model for MHD by Paul Dellar [32,33], and the 3D LBM models for magnetic reconnection and electrodynamics by M. Mendoza *et al.* [39,40]. All these models based on Navier-Stokes equations and magnetic diffusion equations have displayed the powerful simulation ability of LBM and supplied many useful results of plasma physics, and will get further development in future, though their mathematic model is a macroscopic approximation of microscopic collective dynamics of charged particles. From another point of view the plasma LBM simulation can be done directly, based on Boltzmann-Maxwell kinetics equations, because kinetics description is a more intrinsic physical model. Checking this model carefully, we find it is a multicomponent, multiscale flow problem with complicated interactions between self-consistent field and charged particles. For this purpose, hyperfine collision and force models should be structured and a suitable electromagnetic numerical method should be introduced. Several collision models had been studied for multicomponent flow, such as the initiating work by Flekkøy [42], the pseudopotential model and its improvement by X. Shan *et al.* [43], and the free energy model by M. R. Swift *et al.* [44]. Among the many works on collision models for multicomponent flow, a group called kinetics models deserves special attention for the present work. They describe binary mixture collisions directly from kinetics theory, which are physical and universal. A kind of multicomponent collision models based on Hamei kinetics for mixtures were developed by P. Asinari and L. S. Luo [45,46]. Simple binary mixture force models could be found in their papers as well. As a modification, some finer force models designed for single-component flow should be used in these multicomponent models, such as the one proposed by X. He *et al.* [47] and its equivalent form proposed by Z. Guo *et al.* [48]. When it comes to electromagnetic numerical methods, choices are abundant, as FEM, FVM, and method of moment (MoM) are all popular in this regime. Considering the demand in

time-domain calculation and the compatibility with LBM, we chose the finite-difference time-domain (FDTD) method for self-consistent field simulation [49,50].

The first 2D hybrid LBM and FDTD method for plasmas was developed by Huayu Li and Hyungson Ki [51–53]. They structured the framework of the model and proved its veracity by numerical tests. Recently a modified model had been proposed by them for laser plasma interaction (LPI), which considered the impact ionization and three-body recombination [53]. Their works were improved by other researchers as well, such as the modified LPI model introduced by X. Zhang *et al.* [54]. All these models only consider the collisions between neutrals as an approximation and the force terms could be improved for the multicomponent flow model. In this paper, we present a FDTD-LBM model for electromagnetic wave propagation in weakly ionized hydrogen plasmas, which consists of elastic collision terms between molecules, Coulomb collision terms between charged particles, kinetics collision, and force models in multicomponent schemes and multiscale lattice technique for matching FDTD to LBM. The FDTD-LBM model has second-order accuracy and a large stable range.

Section II describes the physical model, with the unified three-component collision and force terms approximation schemes, plus the formulations of elastic and Coulomb collisions. The schemes of multicomponent local equilibrium distribution functions are developed in Appendix A. Section III describes the numerical model, including the distribution of physical variables, stability condition, lattice interpolation method, filtering techniques, and computational procedure. The discretization schemes are developed in Appendix B. In Sec. IV, a series of simulations have been implemented to validate the model. The main results and discussions are presented in this section.

II. PHYSICAL MODEL

A. Review of the Maxwell-Boltzmann equations

In this paper, two assumptions are used. First, the plasmas considered consist of three components, which are electrons, ions, and neutrals. Second, there are no elastic collisions, such as ionization and recombination, in these dynamics.

Assuming the kinetics model, the evolution of the weakly ionized plasma can be described by the Boltzmann-Maxwell equations [5,16]

$$
\frac{\partial}{\partial t} f^{(e)} + \vec{V}_e \cdot \vec{\nabla} f^{(e)} + \frac{Q_e}{m_e}(\vec{E} + \vec{V}_e \times \vec{B}) \cdot \vec{\nabla}_{Ve} f^{(e)}
$$
$$
= \left[\frac{\partial}{\partial t} f^{(e)}\right]_{ee} + \left[\frac{\partial}{\partial t} f^{(e)}\right]_{ei} + \left[\frac{\partial}{\partial t} f^{(e)}\right]_{en} \quad (1)
$$

$$
\frac{\partial}{\partial t} f^{(i)} + \vec{V}_i \cdot \vec{\nabla} f^{(i)} + \frac{Q_i}{m_i}(\vec{E} + \vec{V}_i \times \vec{B}) \cdot \vec{\nabla}_{Vi} f^{(i)}
$$
$$
= \left[\frac{\partial}{\partial t} f^{(i)}\right]_{ie} + \left[\frac{\partial}{\partial t} f^{(i)}\right]_{ii} + \left[\frac{\partial}{\partial t} f^{(i)}\right]_{in} \quad (2)
$$

$$
\frac{\partial}{\partial t} f^{(n)} + \vec{V}_n \cdot \vec{\nabla} f^{(n)}
$$
$$
= \left[\frac{\partial}{\partial t} f^{(n)}\right]_{ne} + \left[\frac{\partial}{\partial t} f^{(n)}\right]_{ni} + \left[\frac{\partial}{\partial t} f^{(n)}\right]_{nn} \quad (3)
$$

$$\vec{\nabla} \times \vec{E} = -\frac{\partial}{\partial t}\vec{B} \tag{4}$$

$$\vec{\nabla} \times \vec{H} = \frac{\partial}{\partial t}\vec{D} + \vec{J} \tag{5}$$

$$\vec{\nabla} \cdot \vec{D} = \sigma_f \tag{6}$$

$$\vec{\nabla} \cdot \vec{B} = \vec{0} \tag{7}$$

$$\sigma_f = \int (Q_e f_e + Q_i f_i)\, d\vec{V} \tag{8}$$

$$\vec{J} = \int (Q_e f_e + Q_i f_i)\,\vec{V} d\vec{V} \tag{9}$$

$$\vec{D} = \varepsilon_0 \vec{E} \tag{10}$$

$$\vec{B} = \mu_0 \vec{H}. \tag{11}$$

In the preceding equations, $f^{(s)}(\vec{x},\vec{V},t)$ is the single-particle distribution function in phase space, where $s = e,i,n$ denotes the type of particles and can take e,i,n for electrons, ions and neutrals. $\vec{V}_s$ is the macroscopic velocity and m_s is the mass of different type of particle. $Q_e = -e$ is the charge of the electron and $Q_i = Ze$ is the charge of the ion. σ_f and $\vec{J}$ are free charge density and transport electric current density in plasma area.

$[\frac{\partial}{\partial t} f^{(s)}]_{ss'}$ represents the change rate of $f^{(s)}$ caused by collision interactions between the two types of components of s and s'. $\frac{Q_s}{\mathrm{m}_s}(\vec{E} + \vec{V}_s \times \vec{B})$ represents the acceleration of s component driven by self-consistent field.

Equations (1)–(3) describe the transport movement of plasma components. Equations (4)–(7) describe the evolution of self-consistent field. The nonlinear coupled relation between field and particles is represented by Eqs. (8) and (9).

Equations (10) and (11) are electromagnetic constitutive relationships.

B. Velocity discretization and Bhatnagar-Gross-Krook approximation

A norm lattice Boltzmann model consist of three elements, which are discrete velocity model (DVM), equilibrium distribution function, and evolution equation. Appropriative distribution function is the key part of the model and its embodiment depends on DVM.

The D2Q9 model is a widely used DVM proposed by Y. H. Qian *et al.* [55]. In this model the local equilibrium distribution function in subspaces is defined as the first approximation of the Boltzmann distribution

$$f_\alpha^{(s,eq)} = n_s \omega_\alpha \left[1 + \frac{\vec{e}_\alpha^{(s)} \cdot \vec{V}_s}{\theta_s^2} + \frac{(\vec{e}_\alpha^{(s)} \cdot \vec{V}_s)^2}{2\theta_s^4} - \frac{V_s^2}{2\theta_s^2} \right]. \tag{12}$$

In Eq. (12), subscript α denote nine subspaces, which are related to nine different velocities. n_s is the number density and θ_s is the sound velocity of s component. ω_α and $\vec{e}_\alpha^{(s)}$ are weight and velocity vector of the D2Q9 DVM.

$$\omega_\alpha = \begin{cases} 4/9 & \alpha = 0 \\ 1/9 & \alpha = 1,2,3,4 \\ 1/36 & \alpha = 5,6,7,8 \end{cases} \tag{13}$$

$$c_l^s = \sqrt{3}\theta_s \tag{14}$$

$$\theta_s = \sqrt{\frac{k_B T_s}{\mathrm{m}_s}} \tag{15}$$

$$\vec{e}_\alpha^{(s)} = \begin{cases} (0,0), & \alpha = 0 \\ \left(\cos\left[(\alpha-1)\frac{\pi}{2}\right], \sin\left[(\alpha-1)\frac{\pi}{2}\right]\right) c_l^{(s)}, & \alpha = 1,2,3,4 \\ \sqrt{2}\left(\cos\left[(2\alpha-1)\frac{\pi}{4}\right], \sin\left[(2\alpha-1)\frac{\pi}{4}\right]\right) c_l^{(s)}, & \alpha = 5,6,7,8 \end{cases} . \tag{16}$$

In the preceding equations, c_l^s is the lattice sound velocity of the s component, which limits the lattice time step ratio.

The Bhatnagar-Gross-Krook (BGK) approximation is a kind of simplified collision operator, which assumes that the collision interaction that leads to equilibrium could be replaced by a relaxation process [56]. The lattice Boltzmann equations with BGK approximation are described as

$$\begin{aligned} \frac{\partial}{\partial t} f_\alpha^{(e)} + \vec{e}_\alpha^{(e)} \cdot \vec{\nabla} f_\alpha^{(e)} &= -\frac{1}{\tau_e}\left[f_\alpha^{(e)} - f_\alpha^{(e,eq)} \right] + F_\alpha^{(e)} \\ \frac{\partial}{\partial t} f_\alpha^{(i)} + \vec{e}_\alpha^{(i)} \cdot \vec{\nabla} f_\alpha^{(i)} &= -\frac{1}{\tau_i}\left[f_\alpha^{(i)} - f_\alpha^{(i,eq)} \right] + F_\alpha^{(i)} \\ \frac{\partial}{\partial t} f_\alpha^{(n)} + \vec{e}_\alpha^{(n)} \cdot \vec{\nabla} f_\alpha^{(n)} &= -\frac{1}{\tau_n}\left[f_\alpha^{(n)} - f_\alpha^{(n,eq)} \right] \end{aligned} \tag{17}$$

where τ_s, $s = e,i,n$ is the collision relaxation time of s component, which is the inverse of the collision frequency. $F_\alpha^{(e)}$ and $F_\alpha^{(i)}$ are Lorentz force terms in subspaces. Equations (17) are the basic evolution equations of the model.

C. Approximation model of the collision terms in weakly ionized plasmas

The BGK approximation is originally designed for single-component gas [56]. As an improved alternative for the binary kinetics model, several kinetic schemes have been introduced [42–44]. For the purpose of describing complicated interactions in plasmas, we propose the multicomponent collision terms for electron with BGK approximation as

$$\begin{aligned} &\left[\frac{\partial}{\partial t} f_\alpha^{(e)} \right]_{ee} + \left[\frac{\partial}{\partial t} f_\alpha^{(e)} \right]_{ei} + \left[\frac{\partial}{\partial t} f_\alpha^{(e)} \right]_{en} \\ &= -\frac{1}{\tau_{ee}}\left[f_\alpha^{(e)} - f_\alpha^{(ee,eq)} \right] \\ &\quad -\frac{1}{\tau_{ei}}\left[f_\alpha^{(e)} - f_\alpha^{(ei,eq)} \right] - \frac{1}{\tau_{en}}\left[f_\alpha^{(e)} - f_\alpha^{(en,eq)} \right] \end{aligned}$$

$$= -\frac{\tau_{ei}\tau_{en} + \tau_{ee}\tau_{en} + \tau_{ee}\tau_{ei}}{\tau_{ee}\tau_{ei}\tau_{en}}$$

$$\times \left[f_\alpha^{(e)} - \frac{\tau_{ei}\tau_{en}}{\tau_{ei}\tau_{en} + \tau_{ee}\tau_{en} + \tau_{ee}\tau_{ei}} f_\alpha^{(ee,eq)} \right.$$

$$- \frac{\tau_{ee}\tau_{en}}{\tau_{ei}\tau_{en} + \tau_{ee}\tau_{en} + \tau_{ee}\tau_{ei}} f_\alpha^{(ei,eq)}$$

$$\left. - \frac{\tau_{ee}\tau_{ei}}{\tau_{ei}\tau_{en} + \tau_{ee}\tau_{en} + \tau_{ee}\tau_{ei}} f_\alpha^{(en,eq)} \right], \qquad (18)$$

where $f_\alpha^{(ee,eq)}$, $f_\alpha^{(ei,eq)}$, and $f_\alpha^{(en,eq)}$ are partial local equilibrium distribution functions of electron (for more details see Appendix A). The terms τ_{ee}, τ_{ei}, and τ_{en} are partial collision relaxation times of electron, which rest with different collision types. To simplify Eq. (18), we can define some useful parameters

$$\tau_e = \frac{\tau_{ee}\tau_{ei}\tau_{en}}{\tau_{ei}\tau_{en} + \tau_{ee}\tau_{en} + \tau_{ee}\tau_{ei}} \qquad (19)$$

$$\beta_{ee} = \frac{\tau_{ei}\tau_{en}}{\tau_{ei}\tau_{en} + \tau_{ee}\tau_{en} + \tau_{ee}\tau_{ei}} \qquad (20)$$

$$\beta_{ei} = \frac{\tau_{ee}\tau_{en}}{\tau_{ei}\tau_{en} + \tau_{ee}\tau_{en} + \tau_{ee}\tau_{ei}} \qquad (21)$$

$$\beta_{en} = \frac{\tau_{ee}\tau_{ei}}{\tau_{ei}\tau_{en} + \tau_{ee}\tau_{en} + \tau_{ee}\tau_{ei}} \qquad (22)$$

$$f_\alpha^{(e,eq)} = \beta_{ee} f_\alpha^{(ee,eq)} + \beta_{ei} f_\alpha^{(ei,eq)} + \beta_{en} f_\alpha^{(en,eq)}. \qquad (23)$$

In the preceding equations, τ_e equals the collision relaxation time of electron defined in Eq. (17) and $f_\alpha^{(e,eq)}$ is the local equilibrium distribution function of electron. Then

$$\left[\frac{\partial}{\partial t} f_\alpha^{(e)} \right]_{ee} + \left[\frac{\partial}{\partial t} f_\alpha^{(e)} \right]_{ei} + \left[\frac{\partial}{\partial t} f_\alpha^{(e)} \right]_{en}$$

$$= -\frac{1}{\tau_e} \left[f_\alpha^{(e)} - f_\alpha^{(e,eq)} \right]. \qquad (24)$$

The multicomponent collision terms for ion and neutral could be modeled in the same procedure. Then they are

described as

$$\left[\frac{\partial}{\partial t} f_\alpha^{(i)} \right]_{ie} + \left[\frac{\partial}{\partial t} f_\alpha^{(i)} \right]_{ii} + \left[\frac{\partial}{\partial t} f_\alpha^{(i)} \right]_{in}$$

$$= -\frac{1}{\tau_i} \left[f_\alpha^{(i)} - \beta_{ie} f_\alpha^{(ie,eq)} - \beta_{ii} f_\alpha^{(ii,eq)} - \beta_{in} f_\alpha^{(in,eq)} \right]$$

$$= -\frac{1}{\tau_i} \left[f_\alpha^{(i)} - f_\alpha^{(i,eq)} \right] \qquad (25)$$

$$\left[\frac{\partial}{\partial t} f_\alpha^{(n)} \right]_{ne} + \left[\frac{\partial}{\partial t} f_\alpha^{(n)} \right]_{ni} + \left[\frac{\partial}{\partial t} f_\alpha^{(n)} \right]_{nn}$$

$$= -\frac{1}{\tau_n} \left[f_\alpha^{(n)} - \beta_{ne} f_\alpha^{(ne,eq)} - \beta_{ni} f_\alpha^{(ni,eq)} - \beta_{nn} f_\alpha^{(nn,eq)} \right]$$

$$= -\frac{1}{\tau_n} \left[f_\alpha^{(n)} - f_\alpha^{(n,eq)} \right]. \qquad (26)$$

Equations (24)–(26) supply a hyperfine description for the combined action of different types of collisions (for more details see Appendix A).

D. Approximation model of the Lorentz force

The force term is another essential element of the LBM model. Though there are more than ten kinds of force models that have been developed, all of them are originally designed for single-component flow. Among the many works, the one introduced by Z. Guo *et al.* deserves special attention for the present work, as this model has clear physical connotations and is equal to the one introduced by He *et al.* to secondary-order approximation, which is widely used [47,48].

Based on Eq. (23), the He model in multicomponent form could be written as (take electron component for example)

$$\vec{a}^{(e)} = \frac{Q_e}{m_e}(\vec{E} + \vec{V}_e \times \vec{B}) \qquad (27)$$

$$F_\alpha^{(e)} = [-\vec{a}^{(e)} \cdot \vec{\nabla}_V f^{(e)}]_\alpha \approx [-\vec{a}^{(e)} \cdot \vec{\nabla}_V f^{(e,eq)}]_\alpha$$

$$= [-\vec{a}^{(e)} \cdot \vec{\nabla}_V (\beta_{ee} f^{(ee,eq)} + \beta_{ei} f^{(ei,eq)} + \beta_{en} f^{(en,eq)})_\alpha]. \qquad (28)$$

As an alternative for the preceding equation, the Guo model in multicomponent form is obtained

$$F_\alpha^{(e)} = \beta_{ee}\omega_\alpha n_e \left(1 - \frac{\delta t}{2\tau_{ee}}\right) \left[\frac{\vec{a}^{(e)} \cdot \vec{e}_\alpha^{(e)}}{\theta_e^2} + \frac{(\vec{V}_{ee}\vec{a}^{(e)} + \vec{a}^{(e)}\vec{V}_{ee}) : (\vec{e}_\alpha^{(e)}\vec{e}_\alpha^{(e)} - \theta_e^2\overset{\leftrightarrow}{I})}{2\theta_e^4} \right]$$

$$+ \beta_{ei}\omega_\alpha n_e \left(1 - \frac{\delta t}{2\tau_{ei}}\right) \frac{\rho_e}{\rho_e + \rho_i} \left[\frac{\vec{a}^{(e)} \cdot \vec{e}_\alpha^{(e)}}{\theta_e^2} + \frac{(\vec{V}_{ei}\vec{a}^{(e)} + \vec{a}^{(e)}\vec{V}_{ei}) : (\vec{e}_\alpha^{(e)}\vec{e}_\alpha^{(e)} - \theta_e^2\overset{\leftrightarrow}{I})}{2\theta_e^4} \right]$$

$$+ \beta_{en}\omega_\alpha n_e \left(1 - \frac{\delta t}{2\tau_{en}}\right) \frac{\rho_e}{\rho_e + \rho_n} \left[\frac{\vec{a}^{(e)} \cdot \vec{e}_\alpha^{(e)}}{\theta_e^2} + \frac{(\vec{V}_{en}\vec{a}^{(e)} + \vec{a}^{(e)}\vec{V}_{en}) : (\vec{e}_\alpha^{(e)}\vec{e}_\alpha^{(e)} - \theta_e^2\overset{\leftrightarrow}{I})}{2\theta_e^4} \right]$$

$$= \beta_{ee}F_\alpha^{(ee)} + \beta_{ei}F_\alpha^{(ei)} + \beta_{en}F_\alpha^{(en)}, \qquad (29)$$

where ρ_s, $s = e,i,n$ is the mass density of s component. $\vec{V}_{ss'}$ is the centroidal velocity of s and s' component. Obviously $\vec{V}_{ss'}$ is equal to $\vec{V}_{s's}$. δt is the time step of LBM.

In order to calculate the kinetics equations (17), the macroscopic velocity of charged particle is defined as

$$n_e \vec{V}_e = \sum_\alpha \vec{e}_\alpha^{(e)} f_\alpha^{(e)} + \frac{\delta t}{2} \vec{F}^{(e)}, \qquad (30)$$

where $\vec{F}^{(e)}$ describes the external action caused by acceleration $\vec{a}^{(e)}$. Analyzing Eq. (29), the scheme of $\vec{F}^{(e)}$ is obtained

$$\left(1 - \frac{\delta t}{2\tau_{ee}}\right)\vec{F}^{(ee)} = \sum_{\alpha} \vec{e}_{\alpha}^{(e)} F_{\alpha}^{(ee)} \tag{31}$$

$$\left(1 - \frac{\delta t}{2\tau_{ei}}\right)\vec{F}^{(ei)} = \sum_{\alpha} \vec{e}_{\alpha}^{(e)} F_{\alpha}^{(ei)} \tag{32}$$

$$\left(1 - \frac{\delta t}{2\tau_{en}}\right)\vec{F}^{(en)} = \sum_{\alpha} \vec{e}_{\alpha}^{(e)} F_{\alpha}^{(en)} \tag{33}$$

$$\vec{F}^{(e)} = \beta_{ee}\vec{F}^{(ee)} + \beta_{ei}\vec{F}^{(ei)} + \beta_{en}\vec{F}^{(en)}. \tag{34}$$

The multicomponent force term for ion could be modeled in the same way. Then it is described as

$$\vec{a}^{(i)} = \frac{Q_i}{m_i}(\vec{E} + \vec{V}_i \times \vec{B}) \tag{35}$$

$$\begin{aligned}
F_{\alpha}^{(i)} &\approx [-\vec{a}^{(i)} \cdot \vec{\nabla}_V f^{(i,eq)}]_{\alpha} \\
&= [-\vec{a}^{(i)} \cdot \vec{\nabla}_V (\beta_{ie} f^{(ie,eq)} + \beta_{ii} f^{(ii,eq)} + \beta_{in} f^{(in,eq)})]_{\alpha} \\
&= \beta_{ie} F_{\alpha}^{(ie)} + \beta_{ii} F_{\alpha}^{(ii)} + \beta_{in} F_{\alpha}^{(in)}
\end{aligned} \tag{36}$$

$$\vec{F}^{(i)} = \beta_{ie}\vec{F}^{(ie)} + \beta_{ii}\vec{F}^{(ii)} + \beta_{in}\vec{F}^{(in)} \tag{37}$$

$$n_i\vec{V}_i = \sum_{\alpha} \vec{e}_{\alpha}^{(i)} f_{\alpha}^{(i)} + \frac{\delta t}{2}\vec{F}^{(i)}. \tag{38}$$

Using Eqs. (24)–(26), (29), and (36), kinetics equations (17) could be updated step by step.

E. Physical quantities in the model

There are some physical parameters that should be given before using the LBM model to simulate electromagnetic wave propagation in weakly ionized plasmas. First of all, the initial distribution functions could be defined as uniform and the number densities are obtained by the Saha equation [51]

$$\frac{n_i}{n_n} \approx 3.00 \times 10^{27} T_e^{3/2} \frac{1}{n_i} \exp\left(-\frac{U_i}{T_e}\right), \tag{39}$$

where U_i is the first ionization energy of neutral and for hydrogen it is 15.427 eV (T_e in this equation is defined in eV).

In order to calculate collision terms, different collision relaxation times are necessary parameters. The elastic collision relaxation time is defined as [51]

$$\tau_{ss'} = \frac{1}{\sigma_{ss'}n_{s'}\theta_s} \tag{40}$$

$$\sigma_{ss'} = \pi(r_s + r_{s'})^2, \tag{41}$$

where subscript ss' denotes the following five types: en, in, ne, ni, and nn. The $\sigma_{ss'}$ is the collision cross section between s and s' components, then the r_s means particle radius of s component.

The Coulomb collisions between charged particles are active in a kind of long-distance interaction form, which is different from the elastic collision. With Landau approximation, the ei and ii Coulomb collisions relaxation times are described as [5]

$$\tau_{ei} = \frac{T_e^{3/2}\sqrt{m_e}}{4\pi Q_e^2 Q_i^2 n_i L_e} \tag{42}$$

$$\tau_{ii} = \frac{T_i^{3/2}\sqrt{m_i}}{4\pi Q_i^4 n_i L_i}, \tag{43}$$

where L_e and L_i are Coulomb logarithms for electron and ion and they are defined as [5]

$$L_e = \ln\left(\frac{T_e^{3/2}}{\sqrt{4\pi n_e}Q_e^2 Q_i}\right) \tag{44}$$

$$L_i = \ln\left(\frac{T_i^{3/2}}{\sqrt{4\pi n_i}Q_i^2 |Q_e|}\right). \tag{45}$$

With the same definition, τ_{ee} and τ_{ie} could be obtained. Comparing them with τ_{ei} and τ_{ii}, we have the following results [5]

$$\tau_{ee} \sim \tau_{ei} \tag{46}$$

$$\tau_{ie} \gg \tau_{ii}. \tag{47}$$

Equations (46) and (47) are useful in approximation simulation.

Coulomb collision frequencies are usually too low compared with elastic collisions so that many models neglect them to simplify the calculation. But as a complete theoretical description, Coulomb collisions should be included in the LBM model. Actually Coulomb collisions could have the same strength with elastic collisions in some critical situations.

With the LBM simulation, some physical quantities could be obtained and they are updated step by step, such as number density, mass density, charge density, macroscopic velocity, current density, and centroidal velocity, which are defined as

$$n_s = \sum_{\alpha} f_{\alpha}^{(s)} \tag{48}$$

$$\rho_s = \sum_{\alpha} m_s f_{\alpha}^{(s)} \tag{49}$$

$$\sigma_f = \sum_{\alpha,s} Q_s f_{\alpha}^{(s)} \tag{50}$$

$$n_n\vec{V}_n = \sum_{\alpha} \vec{e}_{\alpha}^{(n)} f_{\alpha}^{(n)} \tag{51}$$

$$\vec{J} = \sum_{\alpha,s} Q_s \vec{e}_{\alpha}^{(s)} f_{\alpha}^{(s)} = Q_e n_e \vec{V}_e + Q_i n_i \vec{V}_i \tag{52}$$

$$\vec{V}_{ss'} = \vec{V}_{s's} = \frac{\rho_s \vec{V}_s + \rho_{s'} \vec{V}_{s'}}{\rho_s + \rho_{s'}}. \tag{53}$$

In one part, Eqs. (48)–(53) describe the macroscopic state of the plasmas, which are used for diagnosing. In another, they are necessary for updating evolution equations. For instance, Eq. (52) is used as the source term in the FDTD simulation.

F. Applicability of the model

The FDTD-LBM model presented in this paper is derived from Maxwell-Boltzmann equations (also called Vlasov kinetics equations). Then there are some fundamental hurdles we cannot avoid when LBM-like schemes are used for Vlasov

description. In a Vlasov-type description, strong fields will easily excite higher-order Hermite coefficients. However, LBM-like schemes by definition truncate at finite order (and very small too) Hermite coefficients. Thus, it is obvious that LBM-like schemes can work only in the presence of natural smallness parameters, such as Mach number. This is the intrinsic limitation of the FDTD-LBM model, which determines the applicability of the model.

Taking the strong laser field and plasma interaction for example, we give further explanation for the preceding conclusion. When the field density of incident laser is greater than a certain threshold, obvious nonlinear parametric processes will be observed and some abnormal electromagnetic relation's company with high-order modes is excited. The LBM-like schemes cannot sufficiently describe these phenomena, for they only consider low-order terms near equilibrium state. In other words, the FDTD-LBM model cannot describe nonlinear parametric processes sufficiently.

When it comes to PST, the field density of incident electromagnetic waves is far lower than strong laser and the collision absorption is the main physical mechanism, which leads to equilibrium state. Then Mach number in this problem is very small. As a result, The FDTD-LBM model presented in this paper is suitable to describe electromagnetic wave propagation in weakly ionized plasmas.

III. NUMERICAL MODEL

Once the parameters are selected, the FDTD-LBM model can be used for electromagnetic wave weakly ionized plasma interaction. Based on the physical model presented in Sec. II, the numerical model is obtained. Figure 1 shows the simulation domain.

In this study, the FDTD simulation domain for electromagnetic wave computation is discretized by a 500×250 uniform Yee grid, which is surrounded by a convolution perfect matched layer (CPML) boundary in the X direction to simulate free space [57–60]. The CPML thickness is 10 layers. The LBM simulation domain for the kinetics equation computation is discretized by an 800×500 uniform lattice whose scalar is half of the Yee grids. The mixed boundary is used in the X direction for LBM computation. In order to simulate infinite boundary, the periodic boundary is introduced both for FDTD and LBM in the Y direction. Assuming that the electromagnetic wave is in TM mode whose field quantities are
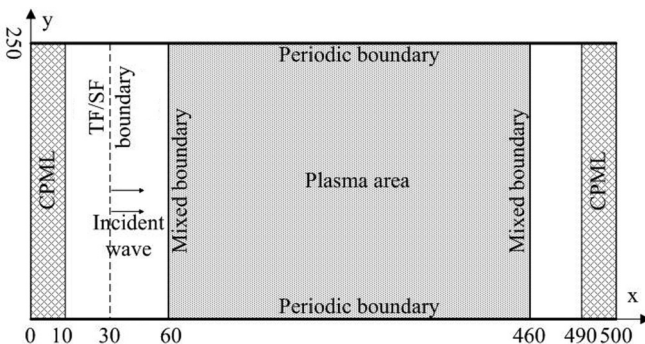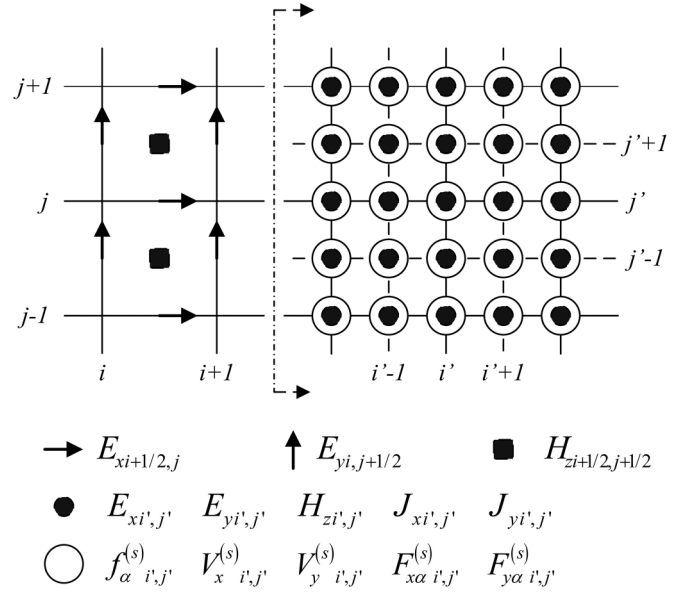

FIG. 2. Variables positions in the simulation domain.

E_x, E_y, and H_z, the total field scatter field (TF-SF) boundary is used to introduce uniform incident wave.

To enhance computation accuracy and simplify sampling procedure, subgrids are introduced in the public domain (coincide with the uniform lattices), where FDTD variables are interpolated into subgrids. Figure 2 shows all physical variables distributions in the simulation domain.

The preceding schematic shows the distributions of all kinds of physical variables in every area. The left area is the FDTD domain. In this area the electric and magnetic field variables are distributed according to the normal 2D Yee's rule. The right area is the public domain where the public subgrid scalar is half of the Yee grid scalar in FDTD domain and all kinds of variables are distributed on every node. It is obvious that the physical variables in public domain cannot be obtained directly. To obtain FDTD variables, the linear interpolation technique is used, as subgrids are perfectly embedded in the normal Yee grids (for more details see Appendix B). To obtain LBM variables, the cubic spline interpolation technique is introduced, as electromagnetic wave phase velocity is far grater than lattice sound velocity so that subgrid scalar is far larger than normal LBM lattice scalar. More details are discussed later.

Numerical stability is an essential problem in all kinds of numerical simulations. The stability of explicit FDTD scheme is controlled by the Courant-Friedricks-Lewy (CFL) condition, which is written as

$$\frac{1}{\Delta t} \geqslant c \sqrt{\frac{1}{\Delta x^2} + \frac{1}{\Delta y^2}}, \tag{54}$$

where Δt is the time step and c is the light velocity in vacuum (c should be replaced by c' if the wave propagates in dielectric medium, where c' is the wave phase velocity in medium) [49]. To simplify the calculation, space step $\Delta x = \Delta y$ is usually considered as a basic assumption. Then the subgrid scalar $\Delta x' = \Delta y' = 0.5\Delta x$ can be defined in the public domain. Considering the numerical dispersion, the

FIG. 1. Schematic of the simulation domain.

following conditions are usually used

$$\Delta x \leqslant 0.1\lambda_{\min}, \quad \Delta x = 0.05\lambda_{\min}, \quad \Delta t \leqslant \frac{\Delta x}{2c'}, \quad (55)$$

where $\lambda_{\min}$ is the minimal wave length in simulation domain. Although the CFL condition makes FDTD simulation is stability, it is incompatible with normal LBM model, for normal lattice is limited by

$$\delta x^{(s)} = c_i^{(s)} \delta t^{(s)}, \quad (56)$$

where lattice length $\delta x^{(s)}$ is defined by lattice time step $\delta t^{(s)}$, which is associate with the physical emplastic of plasma [18]

$$\upsilon = \theta_s^2 (\tau_s - 0.5\delta t^{(s)}), \quad (57)$$

where υ is decided by component temperature and collision frequency. The preceding equation shows that $\delta t^{(s)}$ introduces numerical emplastic. Considering the statistical fluctuation, υ is allowed finite variational to extend the simulation. With this assumption, non-negative is a basic limitation to υ, otherwise the computation will be unstable. Once the physical emplastic and lattice time step are decided, modified relaxation time for LBM can be obtained. When the lattice time step $\delta t^{(s)}$ is far smaller than physical relaxation time, the modification can be ignored according to Eq. (57).

Based on preceding discussion, the problem that CFL condition is incompatible with normal LBM needs to be solved. For this purpose, two techniques should be considered. First, the multi-time-step method is widely used in PIC simulation to solve multicomponent problems. Second, the interpolation method has been used in LBM model to simulate the high Reynolds number problem. In this study, the second technique is selected, as it is more suitable for large scalar simulation. Then the following relations are defined to construct the interpolation model

$$\delta t^{(s)} = \Delta t \quad (58)$$

$$r_x^{(s)} = r_y^{(s)} = \frac{\delta x^{(s)}}{\Delta x'}. \quad (59)$$

With Eqs. (58) and (59), cubic spline interpolation could be introduced to update distribution functions

$$f_{\alpha,i+\delta x^{(s)}}^{(s)t+\frac{3}{2}} \to f_{\alpha,i}^{(s)t+\frac{3}{2}}. \quad (60)$$

The cubic spline has a more smooth character than quadratic polynomial interpolation described as

$$f_{\alpha,i}^{(s)t+\frac{3}{2}} = f_{\alpha,i+\delta x^{(s)}-1}^{(s)t+\frac{3}{2}} \frac{r_x^{(s)}\left(1+r_x^{(s)}\right)}{2} + f_{\alpha,i+\delta x^{(s)}}^{(s)t+\frac{3}{2}}\left(1-r_x^{(s)}\right)$$

$$\times \left(1+r_x^{(s)}\right) + f_{\alpha,i+\delta x^{(s)}+1}^{(s)t+\frac{3}{2}} \frac{r_x^{(s)}\left(r_x^{(s)}-1\right)}{2}. \quad (61)$$

With the interpolation lattice scheme, considering the CFL condition and physical emplastic conditions, a self-consistent numerical method for 2D plasma electromagnetic wave interaction is developed.

The computational procedure is carried out step by step from FDTD to LBM, which is shown in the following (Fig. 3).

In the preceding flow chart, the stop condition is that both the electromagnetic wave and the plasma reach steady state. If wave frequency is far lower than electron-neutral collision frequency, the time step is far grater than physical relaxation
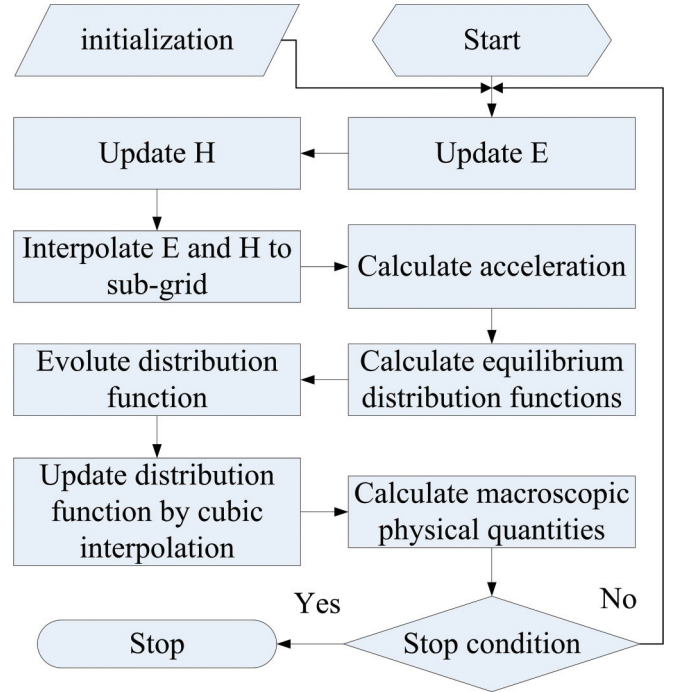

FIG. 3. Flow chart of the FDTD-LBM simulation.

time, and then relatively fewer steps can lead the system to steady state. On the contrary, if wave frequency is far greater than electron-neutral collision frequency, the time step is far smaller than the physical relaxation time, then relatively greater steps (about hundreds of times the physical relaxation time) are needed to keep system in steady state. Based on the procedure, discretization schemes for simulation are obtained (for more details see Appendix B).

There is a detail that should be paid attention to. Physical quantities obtained by interpolation from Yee grid to subgrid are usually polluted by high-frequency numerical white noise. In order to enhance computational accuracy, the mean filtering technique is introduced in this study, which can denoise the physical quantities effectively.

IV. RESULTS AND DISCUSSION

In order to validate our model, several simulations have been implemented. For this purpose, we introduce a simplified analytical model to test our numerical results. We compare the numerical and approximate analytical propagation constants, attenuation constants, and propagation wave forms at different electromagnetic wave frequencies.

As a simplified model, the process of electromagnetic wave propagation in cold weakly ionized plasma gas can be described in fluid dynamics approximation. Due to the ion mass being much greater than the electron mass, the electron Langmuir frequency is much greater than the ion Langmuir frequency. As a result, the relative permittivity of plasma can be written as [5]

$$\varepsilon_r = 1 - \frac{\omega_p^2}{\omega(\omega - j\nu_{en})} = 1 - \frac{\omega_p^2}{\omega^2 + \nu_{en}^2} - j\frac{\nu_{en}\omega_p^2}{\omega(\omega^2 + \nu_{en}^2)}. \quad (62)$$

In Eq. (62), ω is the angular frequency of incident wave, ν_{en} is the electron-neutral collision frequency and ω_p is the electron Langmuir frequency, which is defined as [6]

$$\omega_p = \sqrt{\frac{n_e e^2}{m_e \varepsilon_0}}. \tag{63}$$

With the preceding relative permittivity, we plug the plan wave mode into Maxwell equations, then the frequency dispersion relation could be obtained,

$$k^2 = k_0^2(\varepsilon_r' - j\varepsilon_r''), \tag{64}$$

where k is the mode of wave vector in plasma and k_0 is the wave number in vacuum. ε_r' and ε_r'' are real and imaginary parts of ε_r in plasma.

The complex wave vector k can be rewritten as sum of real part β and imaginary part α

$$k = \beta - j\alpha, \tag{65}$$

where α and β are called the attenuation constant and propagation constant. After plugging Eq. (65) into Eq. (64), we obtain the following schemas:

$$\alpha = k_0\sqrt{\frac{1}{2}\left[\varepsilon_r' + \sqrt{\varepsilon_r'^2 + \varepsilon_r''^2}\right]} = k_0\sqrt{\frac{1}{2}\left[1 - \frac{\omega_p^2}{\omega^2 + \nu_{en}^2} + \sqrt{\left(1 - \frac{\omega_p^2}{\omega^2 + \nu_{en}^2}\right)^2 + \left(\frac{\nu_{en}\omega_p^2}{\omega(\omega^2 + \nu_{en}^2)}\right)^2}\right]} \tag{66}$$

$$\beta = k_0\sqrt{\frac{1}{2}\left[-\varepsilon_r' + \sqrt{\varepsilon_r'^2 + \varepsilon_r''^2}\right]} = k_0\sqrt{\frac{1}{2}\left[\frac{\omega_p^2}{\omega^2 + \nu_{en}^2} - 1 + \sqrt{\left(1 - \frac{\omega_p^2}{\omega^2 + \nu_{en}^2}\right)^2 + \left(\frac{\nu_{en}\omega_p^2}{\omega(\omega^2 + \nu_{en}^2)}\right)^2}\right]}. \tag{67}$$

The preceding equations (66) and (67) indicate that collision plasma is a kind of complicated dissipative and dispersive medium, for attenuation constant α and propagation constant β depend on the frequency of the incident wave.

As the first validation, hydrogen plasma with a 9.5×10^{-5} ionization degree is considered. In this simulation, the temperature of electrons is 0.6 eV and the temperature of ions and neutrals is 0.0253 eV as constants. The number densities of three species are $n_e = n_i = 1.0000 \times 10^{20}$ m^{-3} and $n_n = 1.0522 \times 10^{24}$ m^{-3} according to the Saha equation (39). The corresponding electron Langmuir frequency and electron-neutral collision frequency are $\omega_p = 5.6415 \times 10^{11}$ rad·s^{-1} and $\nu_{en} = 4.2831 \times 10^{11}$ Hz according to Eqs. (63) and (40). Using the preceding parameters we can obtain the theoreticaldispersion relation of this plasma according to Eqs. (64)–(67). Figure 4 shows the dispersion curve of the plasma.

In the preceding curves, we can see that when the incident wave frequency ω is higher than ω_p, the propagation constant ratio $\beta/k_0 \approx 1$ and the attenuation constant α is small. This means that the plasma behaves like a low-loss dispersive dielectric medium, which is important in the PST. On the contrary, when incident wave frequency ω is far lower than ω_p and ν_{en}, the plasma behaves more like a perfect conductor, which leads to strong loss and high reflection.

The incident wave frequencies in this simulation are selected at 1×10^{11}, 2×10^{11}, 3×10^{11}, 4×10^{11}, 5×10^{11}, 6×10^{11}, and 7×10^{11}. All these frequencies are measured by Hz. The amplitude of incident wave is 100 V·m^{-1}. Figures 5–7 show the E_y, H_z, and J_y components sampled at 3×10^{11} Hz when time is 280 17 steps (1000 times τ_e).

In the preceding images, components sampled at 3×10^{11} Hz show that the incident wave is attenuated in the plasma area, and keep uniform in the Y direction. Once the incident wave crosses the plasma-vacuum interface, it will drive the charged particles. Then these particles will depart from the equilibrium center and be accelerated by the time-varying electric field. During this process, strong elastic collisions and somewhat weaker Coulomb collisions exist, which hold a prominently dominant position of the dissipation mechanism. With these collisions, the macroscopic kinetic energy of charged particles acquired from incident electromagnetic wave transfer to thermal energy. This process is usually called energy thermalization.

Figure 8 shows the E_y component sampled at 3×10^{11} Hz along the propagation direction when time is 280 17 steps. From this curve, we can obtain the propagation and attenuation constants and then compare them with the approximate analytical ones.
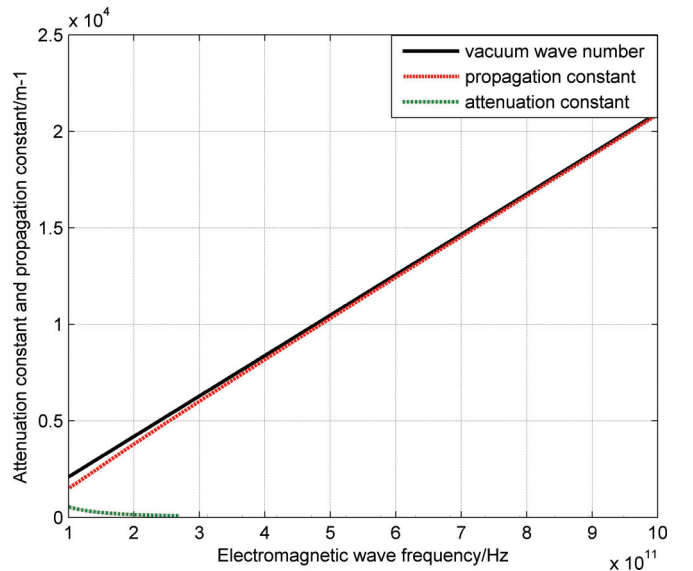

FIG. 4. (Color online) Theoretical dispersion curve of the plasma (the frequencies are from 1×10^{11} to 1×10^{12} Hz).
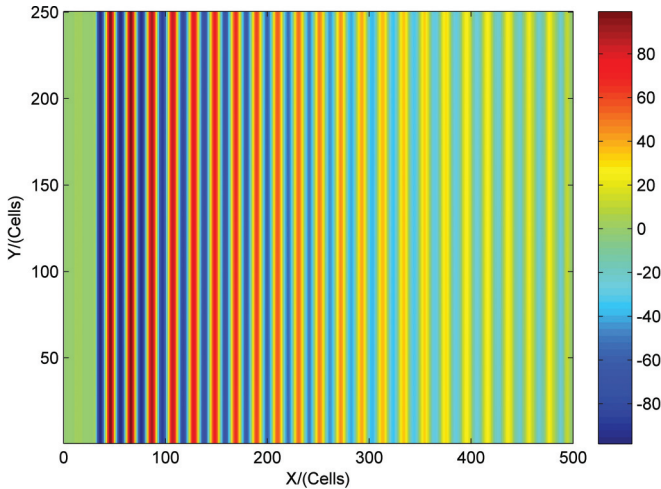
FIG. 5. (Color online) E_y component sampled at 3×10^{11} Hz ($t = 280\,17$ steps), which is measured by V·m^{-1}.

As can be seen from the preceding figure, when the incident wave enters the plasma area, its wave length is increased and its amplitude exponential decays along the propagation direction. These phenomena show that the propagation constant in the plasma area is slightly lower than the vacuum wave number and the attenuation constant is small. The simulations at other frequencies are implemented also. Figure 9 shows the comparison of the propagation and attenuation constants between numerical and approximate analytical results.

The preceding curves show that the numerical propagation and attenuation constants are consistent with the approximate analytical ones, which demonstrates that the model is accurate and can obtain satisfying numerical solutions successfully. Slight deviations come from the numerical errors and the simplification used in analytical model, asonly electron-neutral collision is considered in analytical approximation. Different from macroscopic methods, more parameters of the plasma can be obtained from the distribution functions in this simulation.
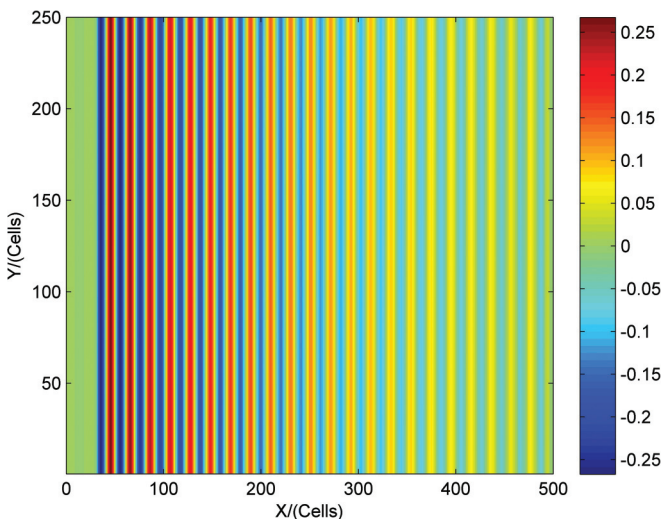

FIG. 6. (Color online) H_z component sampled at 3×10^{11} Hz ($t = 280\,17$steps), which is measured by A·m^{-1}.
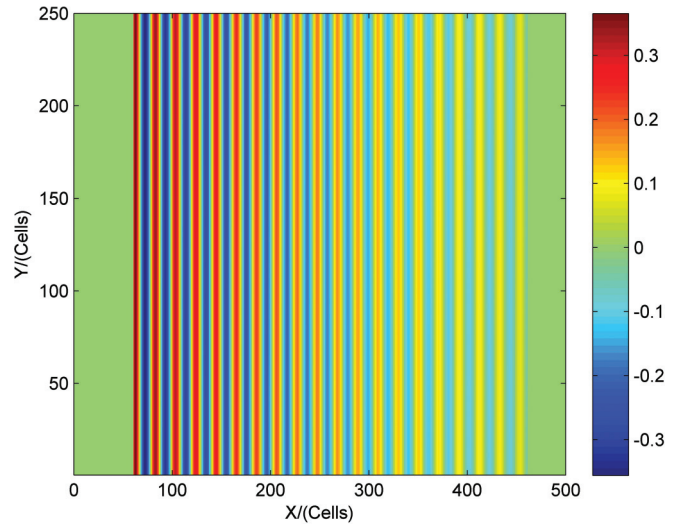

FIG. 7. (Color online) J_y component sampled at 3×10^{11} Hz ($t = 280\,17$ steps), which is measured by A.

Finally, another simulation with hydrogen plasma with 9.1×10^{-4} ionization degree is implemented to support the preceding conclusion. The temperature of electrons is 0.8 eV and the temperature of ions and neutrals is 0.0253 eV as constants. The number densities of three species are $n_e = n_i = 1.0000 \times 10^{22}$ m^{-3}, and $n_i = 1.1043 \times 10^{25}$ m^{-3}. The corresponding electron Langmuir frequency and electron-neutral collision frequency are $\omega_p = 5.6415 \times 10^{12}$ rad·s^{-1} and $\nu_{en} = 5.1905 \times 10^{12}$ Hz. The incident wave frequencies in this simulation are selected at 2×10^{12}, 3×10^{12}, 4×10^{12}, 5×10^{12}, 6×10^{12}, 7×10^{12}, 8×10^{12}, and 9×10^{12}. All these frequencies are measured by Hz. Figure 10 shows the comparison of the propagation and attenuation constants between numerical and approximate analytical results.

The comparison between numerical and approximate analytical results shows that the preceding conclusion is valid and the FDTD-LBM model can accurately simulate the physical
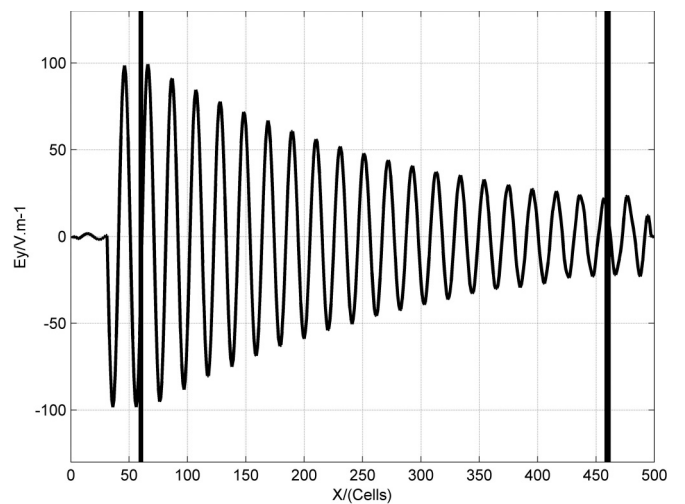

FIG. 8. E_y component sampled on 3×10^{11} Hz along the propagation direction ($t = 280\,17$ steps), plasma region is between the two thick lines.
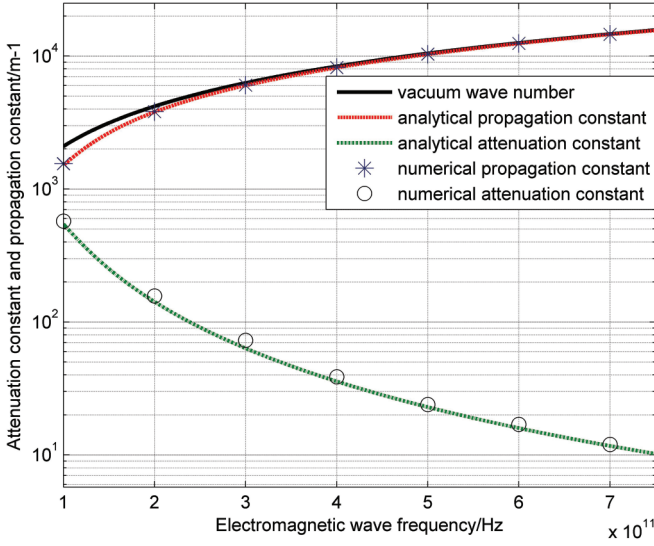
FIG. 9. (Color online) propagation and attenuation constants: numerical versus approximate analytical ($\nu_{en} = 4.2831 \times 10^{11}$ Hz, $\omega_p = 5.6415 \times 10^{11}$ rad·s^{-1}).

phenomena that an electromagnetic wave propagation in weakly ionized hydrogen plasmas.

V. CONCLUSION

In this work, a hybrid electrodynamics and kinetics numerical model has been developed for electromagnetic wave propagation in weakly ionized hydrogen plasmas. The FDTD-LBM model is proved effective to simulate the weakly ionized plasma problems. To our knowledge, the multicomponent BGK collision model considering all kinds of particles collisions (including elastic collisions and Coulomb collisions) and multicomponent force model based on the Guo model are introduced in the FDTD-LBM model, which supplies a hyperfine description on the interactions between electromagnetic wave and weakly ionized plasmas. Cubic
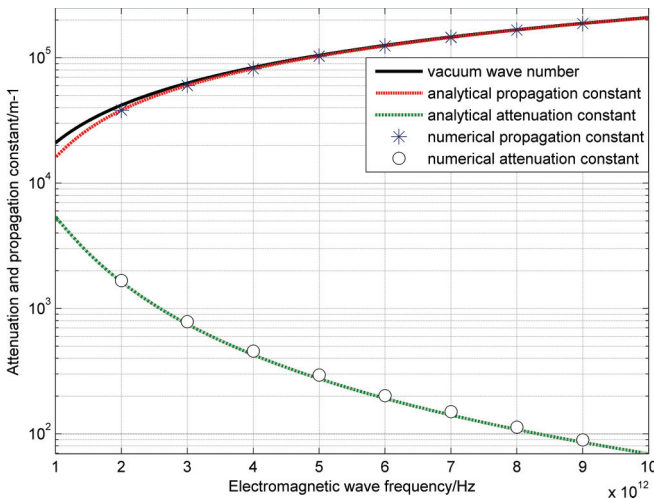

FIG. 10. (Color online) propagation and attenuation constants : numerical versus approximate analytical ($\nu_{en} = 5.1905 \times 10^{12}$ Hz, $\omega_p = 5.6415 \times 10^{12}$ rad·s^{-1}).

spline interpolation and mean filtering technique are separately introduced to solve the multiscalar problem and enhance the physical quantities, which are polluted by numerical noise. Several simulations are implemented to validate the numerical method. The numerical propagation and attenuation constants at different frequencies with different plasma parameters are consistent with the approximate analytical ones, which demonstrate the accuracy of this model. The numerical results show that the plasmas behave like a low-loss dispersive dielectric medium when the incident wave frequencies are higher than the electron Langmuir frequencies. All these results indicate that the weakly ionized plasmas can be used in anti-radar-stealth technique. Additionally, this work can be extended as an effective tool in plasma stealth system design.

APPENDIX A: LOCAL EQUILIBRIUM DISTRIBUTION FUNCTIONS

Partial local equilibrium distribution functions are essential quantities of the multicomponent LBM model established in this study. In order to determine the formulations of this distribution functions, we start by taking the Taylor expansion of the Maxwell distribution function until second order, as follows

$$f_\alpha^{(ee,eq)} = n_e \omega_\alpha \left[1 + \frac{\vec{e}_\alpha^{(e)} \cdot \vec{V}_{ee}}{\theta_e^2} + \frac{(\vec{e}_\alpha^{(e)} \cdot \vec{V}_{ee})^2}{2\theta_e^4} - \frac{V_{ee}^2}{2\theta_e^2} \right] \tag{A1}$$

$$f_\alpha^{(ei,eq)} = n_e \omega_\alpha \left[1 + \frac{\vec{e}_\alpha^{(e)} \cdot \vec{V}_{ei}}{\theta_e^2} + \frac{(\vec{e}_\alpha^{(e)} \cdot \vec{V}_{ei})^2}{2\theta_e^4} - \frac{V_{ei}^2}{2\theta_e^2} \right] \tag{A2}$$

$$f_\alpha^{(en,eq)} = n_e \omega_\alpha \left[1 + \frac{\vec{e}_\alpha^{(e)} \cdot \vec{V}_{en}}{\theta_e^2} + \frac{(\vec{e}_\alpha^{(e)} \cdot \vec{V}_{en})^2}{2\theta_e^4} - \frac{V_{en}^2}{2\theta_e^2} \right] \tag{A3}$$

$$f_\alpha^{(ie,eq)} = n_i \omega_\alpha \left[1 + \frac{\vec{e}_\alpha^{(i)} \cdot \vec{V}_{ie}}{\theta_i^2} + \frac{(\vec{e}_\alpha^{(i)} \cdot \vec{V}_{ie})^2}{2\theta_i^4} - \frac{V_{ie}^2}{2\theta_i^2} \right] \tag{A4}$$

$$f_\alpha^{(ii,eq)} = n_i \omega_\alpha \left[1 + \frac{\vec{e}_\alpha^{(i)} \cdot \vec{V}_{ii}}{\theta_i^2} + \frac{(\vec{e}_\alpha^{(i)} \cdot \vec{V}_{ii})^2}{2\theta_i^4} - \frac{V_{ii}^2}{2\theta_i^2} \right] \tag{A5}$$

$$f_\alpha^{(in,eq)} = n_i \omega_\alpha \left[1 + \frac{\vec{e}_\alpha^{(i)} \cdot \vec{V}_{in}}{\theta_i^2} + \frac{(\vec{e}_\alpha^{(i)} \cdot \vec{V}_{in})^2}{2\theta_i^4} - \frac{V_{in}^2}{2\theta_i^2} \right] \tag{A6}$$

$$f_\alpha^{(ne,eq)} = n_n \omega_\alpha \left[1 + \frac{\vec{e}_\alpha^{(n)} \cdot \vec{V}_{ne}}{\theta_n^2} + \frac{(\vec{e}_\alpha^{(n)} \cdot \vec{V}_{ne})^2}{2\theta_n^4} - \frac{V_{ne}^2}{2\theta_n^2} \right] \tag{A7}$$

$$f_\alpha^{(ni,eq)} = n_n \omega_\alpha \left[1 + \frac{\vec{e}_\alpha^{(n)} \cdot \vec{V}_{ni}}{\theta_n^2} + \frac{(\vec{e}_\alpha^{(n)} \cdot \vec{V}_{ni})^2}{2\theta_n^4} - \frac{V_{ni}^2}{2\theta_n^2} \right]$$
(A8)

$$f_\alpha^{(nn,eq)} = n_n \omega_\alpha \left[1 + \frac{\vec{e}_\alpha^{(n)} \cdot \vec{V}_{nn}}{\theta_n^2} + \frac{(\vec{e}_\alpha^{(n)} \cdot \vec{V}_{nn})^2}{2\theta_n^4} - \frac{V_{nn}^2}{2\theta_n^2} \right].$$
(A9)

The preceding equations (A1)–(A9) represent the partial equilibrium status of test component s in the background component s'. The weighted mean of Eqs. (A1)–(A3) determine the equilibrium distribution function of electron as showed in Eq. (23). With the same procedure, equilibrium distribution functions of ion and neutral are obtained.

APPENDIX B: DISCRETIZATION SCHEMES

Figure 3 shows the computational procedure of the FDTD-LBM model for plasma simulation. In order to carry out this procedure, discretization schemes are developed, as follows

$$E_{xi+1/2,j}^{t+1} = E_{xi+1/2,j}^{t} + \frac{\Delta t}{\varepsilon_0 \Delta y}\left(H_{zi+1/2,j+1/2}^{t+1/2} - H_{zi+1/2,j-1/2}^{t+1/2}\right)$$
$$- \frac{\Delta t}{\varepsilon_0} J_{xi+1/2,j}^{t+1/2}$$
(B1)

$$E_{yi,j+1/2}^{t+1} = E_{yi,j+1/2}^{t} + \frac{\Delta t}{\varepsilon_0 \Delta x}\left(H_{zi-1/2,j+1/2}^{t+1/2} - H_{zi+1/2,j+1/2}^{t+1/2}\right)$$
$$- \frac{\Delta t}{\varepsilon_0} J_{yi,j+1/2}^{t+1/2}$$
(B2)

$$H_{zi+1/2,j+1/2}^{t+3/2}$$
$$= H_{zi+1/2,j+1/2}^{t+1/2} + \frac{\Delta t}{\mu_0 \Delta y}\left(E_{xi+1/2,j+1}^{t+1} - E_{xi+1/2,j}^{t+1}\right)$$
$$+ \frac{\Delta t}{\mu_0 \Delta x}\left(E_{yi,j+1/2}^{t+1} - E_{yi+1,j+1/2}^{t+1}\right).$$
(B3)

Equations (B1)–(B3) are updating equations of TM mode in Yee grid, where the source terms $J_{xi+1/2,j}^{t+1/2}$ and $J_{yi,j+1/2}^{t+1/2}$ are

obtained by Eq. (52) after the LBM calculation.

$$E_{xi+1/2,j}^{t+1/2} = \frac{1}{2}\left(E_{xi+1/2,j}^{t+1} + E_{xi+1/2,j}^{t}\right)$$
(B4)

$$E_{xi,j+1/2}^{t+1/2} = \frac{1}{4}\left(E_{xi+1/2,j}^{t+1/2} + E_{xi+1/2,j+1}^{t+1/2} \right.$$
$$\left. + E_{xi-1/2,j}^{t+1/2} + E_{xi-1/2,j+1}^{t+1/2}\right)$$
(B5)

$$E_{xi,j}^{t+1/2} = \frac{1}{4}\left(E_{xi+1/2,j}^{t+1/2} + E_{xi-1/2,j}^{t+1/2} \right.$$
$$\left. + E_{xi,j+1/2}^{t+1/2} + E_{xi,j-1/2}^{t+1/2}\right)$$
(B6)

$$E_{xi+1/2,j+1/2}^{t+1/2} = \frac{1}{4}\left(E_{xi+1,j+1/2}^{t+1/2} + E_{xi,j+1/2}^{t+1/2} \right.$$
$$\left. + E_{xi+1/2,j+1}^{t+1/2} + E_{xi+1/2,j}^{t+1/2}\right).$$
(B7)

Equations (B4)–(B7) describe the operation of interpolation from Yee grid to subgrid (take E_x for example, the schemes of E_y and H_z can be obtained with the same procedure). After these operations, $E_{xi',j'}^{t+1/2}$, $E_{yi',j'}^{t+1/2}$, and $H_{zi',j'}^{t+1/2}$ on LBM lattice nodes are obtained. As mentioned, mean filtering should be done in this procedure.

$$a_{x\,i',j'}^{(s)t+1/2} = \frac{Q_s}{m_s}\left(E_{xi',j'}^{t+1/2} + \mu_0 V_{s,yi',j'}^{t+1/2} H_{zi',j'}^{t+1/2}\right)$$
(B8)

$$a_{y\,i',j'}^{(s)t+1/2} = \frac{Q_s}{m_s}\left(E_{yi',j'}^{t+1/2} - \mu_0 V_{s,x\,i',j'}^{t+1/2} H_{zi',j'}^{t+1/2}\right).$$
(B9)

Equations (B8) and (B9) are discretization expansions of the accelerations caused by Lorentz force, which are essential terms in the LBM force model.

$$f_{\alpha\,(i',j')+\alpha^{(s)}\Delta t}^{(s)t+3/2} = \left(1 - \frac{\Delta t}{\tau_s}\right)f_{\alpha\,i',j'}^{(s)t+1/2} + \frac{\Delta t}{\tau_s}f_{\alpha\,i',j'}^{(s,eq)t+1/2}$$
$$+ F_{\alpha\,i',j'}^{(s)t+1/2}\Delta t.$$
(B10)

The preceding equation describes the evolution procedure of the distribution functions. After this operation, cubic spline interpolation can be done to update the distribution functions.

Finally, Eqs. (B1)–(B3) and (B10) determine the evolution of the self-consistent field and plasma. These are the discretization equations of hybrid electrodynamics and kinetics.

[1] D. J. Gregoire, J. Santoru, and R. W. Schumacher, Hughes Research Labs Report No. ADA250710, 1992 (unpublished).

[2] J. R. Roth, Hughes Research Labs Report No. ADA285496, 1996 (unpublished).

[3] A. B. Petrin, IEEE Trans. Plasma Sci. **26**, 150 (1998).

[4] B. J. Hu and G. Wei, IEEE Trans. Plasma Sci. **29**, 1 (2001).

[5] E. M. Lifshitz and L. P. Pitaevskii, *Physical Kinetics* (Pergamon Press, New York, 1981).

[6] H. Alfvén *et al.*, *Cosmical Electrodynamics* (Oxford University Press, Oxford, 1963).

[7] T. J. M. Boyd and J. J. Sanderson, *The Physics of Plasmas* (Cambridge University Press, Cambridge, 2003).

[8] C. K. Birdsall and A. B. Langdon, *Plasma Physics via Computer Simulation* (Adam Hilger, Bristol, 1991).

[9] R. W. Hockney and J. W. Eastwood, *Computer Simulation Using Particles* (IOP, Bristol, 1994).

[10] O. Buneman, Phys. Rev. **115**, 503 (1959).

[11] J. M. Dawson *et al.*, Phys. Rev. Lett. **50**, 1455 (1983).

[12] Shao Fuqiu, J. Phys. Soc. Jpn. **69**, 441 (2000).

[13] G. K. Parks, *Physics of Space Plasma: An Introduction*, 2nd ed. (Addison-Wesley, Redwood City, 2004).

[14] V. Malka *et al.*, Nature Phys. **4**, 447 (2008).

[15] L. D. Landau and E. M. Lifshitz, *Fluid Mechanics*, 2nd ed. (Pergamon Press, New York, 1987).

[16] L. D. Landau and E. M. Lifshitz, *The Classical Theory of Fields* (Pergamon Press, New York, 1975).

[17] A. Quarteroni and A. Valli, *Numerical Approximation of Partial Differential Equations* (Springer, Berlin, 1994).

[18] S. Succi, *The Lattice Boltzmann Equation for Fluid Dynamics and Beyond* (Oxford University Press, Oxford, 2001).

[19] M. C. Sukop and D. T. J. Thorne, *Lattice Boltzmann Modeling: An Introduction for Geoscientists and Engineers* (Springer, Berlin, 2005).

[20] G. R. McNamara *et al.*, Phys. Rev. Lett. **61**, 2332 (1988).
[21] F. Higuera, S. Succi *et al.*, Europhys. Lett. **9**, 345 (1989).
[22] S. Chen *et al.*, Phys. Rev. Lett. **67**, 3776 (1991).
[23] E. Aharonov *et al.*, Geophys. Res. Lett. **20**, 679 (1993).
[24] D. O. Martinez *et al.*, Phys. Plasmas **1**, 1850 (1994).
[25] Y. H. Qian *et al.*, Annu. Rev. Comput. Phys. **3**, 195 (1995).
[26] S. Chen *et al.*, Comput. Chem. Eng. **19**, 617 (1995).
[27] G. Fogaccia *et al.*, Phys. Rev. E **54**, 4384 (1996).
[28] M. Swift *et al.*, Phys. Rev. E **54**, 5041 (1996).
[29] B. M. Boghosian *et al.*, Phys. Rev. E **57**, 54 (1998).
[30] L. Luo *et al.*, Phys. Rev. E **62**, 4982 (2000).
[31] W. Miller *et al.*, Phys. Rev. Lett. **86**, 3578 (2001).
[32] P. J. Dellar, J. Comput. Phys. **179**, 95 (2002).
[33] P. J. Dellar, Europhys. Lett. **90**, 50002 (2010).
[34] Hudong Chen *et al.*, Science **301**, 633 (2003).
[35] B. R. Osborn, Master thesis, University of Maryland, 2004 (unpublished).
[36] Z. Guo *et al.*, Phys. Rev. E **75**, 036704 (2007).
[37] S. Palpacelli *et al.*, Phys. Rev. E **75**, 066704 (2007).
[38] S. Palpacelli *et al.*, Phys. Rev. E **77**, 066708 (2008).
[39] M. Mendoza *et al.*, Phys. Rev. E **77**, 026713 (2008).
[40] M. Mendoza *et al.*, Phys. Rev. E **81**, 056708 (2010).
[41] J. Y. Zhang *et al.*, Phys. Rev. E **81**, 066705 (2010).
[42] E. G. Flekkøy, Phys. Rev. E **47**, 4247 (1993).
[43] X. Shan *et al.*, Phys. Rev. E **49**, 2941 (1994).
[44] M. R. Swift *et al.*, Phys. Rev. Lett. **75**, 830 (1995).
[45] P. Asinari, Phys. Rev. E **73**, 056705 (2006).
[46] P. Asinari *et al.*, J. Comput. Phys. **227**, 3878 (2008).
[47] X. He *et al.*, Phys. Rev. E **57**, 13 (1998).
[48] Z. Guo *et al.*, Phys. Rev. E **65**, 046308 (2002).
[49] A. Taflove and S. C. Hagness, *Computational Electrodynamics: The Finite-Difference Time-Domain Method*, 2nd ed. (Artech House, Boston, 2000).
[50] Dennis M. Sullivan, *Electromagnetic Simulation Using The FDTD Method* (IEEE Press, New York, 2000).
[51] H. Li and H. Ki, Phys. Rev. E **76**, 066707 (2007).
[52] H. Li and H. Ki, J. Phys. A **42**, 155501 (2009).
[53] H. Li and H. Ki, Phys. Rev. E **82**, 016703 (2010).
[54] X. Zhang *et al.*, Jpn. J. Appl. Phys. **51**, 01AA04 (2012).
[55] Y. H. Qian *et al.*, Europhys. Lett. **17**, 479 (1992).
[56] P. L. Bhatnagar, E. P. Gross, and M. Krook, Phys. Rev. **94**, 511 (1954).
[57] J. Roden *et al.*, Microw. Opt. Techn. Lett. **27**, 334 (2000).
[58] P. R. Loh *et al.*, Phys. Rev. E **79**, 065601 (2009).
[59] Y. Mao *et al.*, IEEE Antenn. Wirel. Pr. **11**, 164 (2012)
[60] Z. Cai *et al.*, IEEE Microw. Wirel. Co. **22**, 164 (2012).